SIAM J. SCI. COMPUT.
Vol. 27, No. 3, pp. 995–1013

A COMPARISON OF TROUBLED-CELL INDICATORS FOR RUNGE–KUTTA DISCONTINUOUS GALERKIN METHODS USING WEIGHTED ESSENTIALLY NONOSCILLATORY LIMITERS*

JIANXIAN QIU† AND CHI-WANG SHU‡

Abstract. In [*SIAM J. Sci. Comput.*, 26 (2005), pp. 907–929], we initiated the study of using WENO (weighted essentially nonoscillatory) methodology as limiters for the RKDG (Runge–Kutta discontinuous Galerkin) methods. The idea is to first identify "troubled cells," namely, those cells where limiting might be needed, then to abandon all moments in those cells except the cell averages and reconstruct those moments from the information of neighboring cells using a WENO methodology. This technique works quite well in our one- and two-dimensional test problems [*SIAM J. Sci. Comput.*, 26 (2005), pp. 907–929] and in the follow-up work where more compact Hermite WENO methodology is used in the troubled cells. In these works we used the classical minmod-type TVB (total variation bounded) limiters to identify the troubled cells; that is, whenever the minmod limiter attempts to change the slope, the cell is declared to be a troubled cell. This troubled-cell indicator has a TVB parameter M to tune and may identify more cells than necessary as troubled cells when M is not chosen adequately, making the method costlier than necessary. In this paper we systematically investigate and compare a few different limiter strategies as troubled-cell indicators with an objective of obtaining the most efficient and reliable troubled-cell indicators to save computational cost.

Key words. Runge–Kutta discontinuous Galerkin method, limiters, weighted essentially nonoscillatory finite volume scheme, high-order accuracy

AMS subject classifications. 65M60, 65M99, 35L65

DOI. 10.1137/04061372X

1. Introduction.

In [13], we initiated the study of using weighted essentially nonoscillatory (WENO) methodology as limiters for the Runge–Kutta discontinuous Galerkin (RKDG) methods. The idea is to first identify "troubled cells," namely, those cells where limiting might be needed, then to abandon all moments in those cells except the cell averages and reconstruct those moments from the information of neighboring cells using a WENO methodology. This technique works quite well in our one- and two-dimensional test problems [13] and in the follow-up work [14] and [15], where more compact Hermite WENO methodology was used in the troubled cells. In these earlier works we adopted the classical minmod-type total variation bounded (TVB) limiters as in [5, 3, 7] to identify the troubled cells; that is, whenever the minmod limiter attempts to change the slope, the cell is declared to be a troubled cell. This troubled-cell indicator has a TVB parameter M to tune. When M is taken too small, more cells than necessary may be identified as troubled cells. Even though

*Received by the editors August 20, 2004; accepted for publication (in revised form) April 19, 2005; published electronically December 8, 2005.
http://www.siam.org/journals/sisc/27-3/61372.html

†Department of Mathematics, Nanjing University, Nanjing, Jiangsu 210093, People's Republic of China, and Department of Mechanical Engineering, National University of Singapore, Singapore 119260 (jxqiu@nju.edu.cn). This author's research was partially supported by NNSFC grant 10371118 and by NUS research project R-265-000-118-112.

‡Division of Applied Mathematics, Brown University, Providence, RI 02912 (shu@dam.brown.edu). This author's research was partially supported by the Chinese Academy of Sciences while the author was in residence at the University of Science and Technology of China (grant 2004-1-8) and at the Institute of Computational Mathematics and Scientific/Engineering Computing. Additional support was provided by ARO grant W911NF-04-1-0291, NSF grant DMS-0207451, and AFOSR grant F49620-02-1-0113.

the WENO reconstruction procedure used in these cells will not degrade the order of accuracy of the original RKDG scheme, the extra work done for these WENO reconstructions in such wrongly identified troubled cells increases the cost of the algorithm. On the other hand, when M is taken too large, some of the real troubled cells may not be identified, resulting in oscillations or even instability for the method. In this paper we systematically investigate and compare a few different limiter strategies as troubled-cell indicators with an objective of trying to obtain the most efficient and reliable troubled-cell indicators to save the computational cost.

The first discontinuous Galerkin (DG) method was introduced in 1973 by Reed and Hill [16] in the framework of neutron transport (steady-state linear hyperbolic equations). A major development of the DG method was carried out by Cockburn et al. in a series of papers [6, 5, 4, 3, 7], in which they established a framework to easily solve *nonlinear* time-dependent hyperbolic conservation laws,

$$\begin{cases} u_t + \nabla \cdot f(u) = 0, \\ u(x,0) = u_0(x), \end{cases} \tag{1.1}$$

using explicit, nonlinearly stable high-order Runge–Kutta time discretizations [20] and DG discretization in space with exact or approximate Riemann solvers as interface fluxes and TVB limiter [18] to achieve nonoscillatory properties for strong shocks. These schemes are termed RKDG methods.

An important component of RKDG methods for solving conservation laws (1.1) with strong shocks in the solutions is a nonlinear limiter, which is applied to detect discontinuities and control spurious oscillations near such discontinuities. Many such limiters have been used in the literature on RKDG methods. For example, we mention the minmod-type TVB limiter [6, 5, 4, 3, 7], which is a slope limiter using a technique borrowed from the finite volume methodology; the moment-based limiter [1] and an improved moment limiter [2], which are specifically designed for DG methods and work on the moments of the numerical solution. These limiters tend to degrade accuracy when mistakenly used in smooth regions of the solution. More recently, a strategy was designed in [12], based on a strong superconvergence at the outflow boundary of each element in smooth regions for the discontinuous Galerkin method, to detect discontinuities and to lower the order of accuracy in the approximation there to avoid spurious oscillations near such discontinuities when solving hyperbolic systems of conservation laws. There are also many limiters developed in the finite volume and finite difference literature, such as the various flux limiters [23], the monotonicity-preserving (MP) limiters [22], modifications of MP limiters [17], and a discontinuity detecting method [9] used to sharpen contact discontinuities in ENO schemes.

In [13], we initiated a study of using WENO methodology as limiters for RKDG methods. We have adopted the following framework.

Step 1. First we identify the "troubled cells," namely, those cells which might need the limiting procedure.

Step 2. Then we replace the solution polynomials in those troubled cells by reconstructed polynomials using WENO methodology which maintain the original cell averages (conservation), have the same orders of accuracy as before, but are less oscillatory.

This technique works quite well in our one- and two-dimensional test problems in [13] and in the follow-up work [14] and [15], where a more compact Hermite WENO methodology was used in the troubled cells. The emphasis of all these works is on Step 2, where different WENO reconstruction strategies are considered. Step 1 is

dealt with by the classical minmod-type TVB limiters as in [5, 3, 7] to identify the troubled cells. It is realized that the TVB parameter M must be chosen carefully in order to reach a nonoscillatory result with the minimal number of troubled cells. However, Step 1 is not investigated in detail in [13, 14, 15].

We do want to point out a fact, which was also highlighted in [13, 14, 15], that since the WENO reconstruction procedure in Step 2 maintains the high-order accuracy of the original RKDG scheme, it is less crucial for Step 1 to identify exactly the troubled cells. If more troubled cells are identified than necessary, the order of accuracy will not degrade, although the computational cost will increase.

In this paper we concentrate on Step 1 in the procedure above, and investigate systematically a few discontinuity detecting methods as troubled-cell indicators. We also test a new discontinuity detecting method based on the subcell resolution idea of Harten [9]. For Step 2 in the procedure above, we simply use the regular WENO reconstruction procedure developed in [13]. We review and describe the details of a few discontinuity detecting methods in section 2, and present extensive numerical results in section 3 to compare their performance as troubled-cell indicators. Concluding remarks are given in section 4.

2. Review and implementation of discontinuity detecting methods. In this section we review a few discontinuity detecting methods to identify troubled cells. We also develop a new discontinuity detecting method based on the subcell resolution method of Harten [9].

We start with the description in the one-dimensional case and use the notation in [5]; however, we emphasize that the procedure described below does not depend on the specific basis chosen for the polynomials and works also in multidimensions. We would like to solve the one-dimensional scalar conservation law:

$$\begin{cases} u_t + f(u)_x = 0, \\ u(x,0) = u_0(x). \end{cases} \tag{2.1}$$

The computational domain is divided into N cells with boundary points $0 = x_{\frac{1}{2}} < x_{\frac{3}{2}} < \cdots < x_{N+\frac{1}{2}} = L$. The points x_i are the centers of the cells $I_i = [x_{i-\frac{1}{2}}, x_{i+\frac{1}{2}}]$, and we denote the cell sizes by $\Delta x_i = x_{i+\frac{1}{2}} - x_{i-\frac{1}{2}}$ and the maximum cell size by $h = \max_i \Delta x_i$. The solution as well as the test function space are given by $V_h^k = \{p : p|_{I_i} \in P^k(I_i)\}$, where $P^k(I_i)$ is the space of polynomials of degree $\le k$ on the cell I_i. We adopt a local orthogonal basis over I_i $\{v_l^{(i)}(x),\ l = 0, 1, \ldots, k\}$, namely, the scaled Legendre polynomials:

$$v_0^{(i)}(x) = 1, \qquad v_1^{(i)}(x) = \frac{x - x_i}{\Delta x_i/2}, \qquad v_2^{(i)}(x) = \left(\frac{x - x_i}{\Delta x_i/2}\right)^2 - \frac{1}{3}, \ldots .$$

Then the numerical solution $u^h(x,t)$ in the space V_h^k can be written as

$$u^h(x,t) = \sum_{l=0}^{k} u_i^{(l)}(t) v_l^{(i)}(x) \qquad \text{for } x \in I_i, \tag{2.2}$$

and the degrees of freedom $u_i^{(l)}(t)$ are the moments defined by

$$u_i^{(l)}(t) = \frac{1}{a_l} \int_{I_i} u^h(x,t) v_l^{(i)}(x)\, dx, \qquad l = 0, 1, \ldots, k,$$

where $a_l = \int_{I_i} (v_l^{(i)}(x))^2 dx$ are the normalization constants since the basis is not orthonormal. In order to determine the approximate solution, we evolve the degrees of freedom $u_i^{(l)}$:

$$\frac{d}{dt}u_i^{(l)} + \frac{1}{a_l}\left(- \int_{I_i} f(u^h(x,t)) \frac{d}{dx} v_l^{(i)}(x)\, dx + \hat{f}(u^-_{i+1/2}, u^+_{i+1/2}) v_l^{(i)}(x_{i+1/2}) \right. \\ \left. - \hat{f}(u^-_{i-1/2}, u^+_{i-1/2}) v_l^{(i)}(x_{i-1/2}) \right) = 0, \qquad l = 0, 1, \ldots, k, \tag{2.3}$$

where $u^{\pm}_{i+1/2} = u^h(x^{\pm}_{i+1/2}, t)$ are the left and right limits of the discontinuous solution u^h at the cell interface $x_{i+1/2}$, and $\hat{f}(u^-, u^+)$ is a monotone flux (nondecreasing in the first argument and nonincreasing in the second argument) for the scalar case and an exact or approximate Riemann solver for the system case. The semidiscrete scheme (2.3) is discretized in time by a nonlinearly stable Runge–Kutta time discretization, e.g., the third-order version [20]. The integral term in (2.3) can be computed either exactly or by a suitable numerical quadrature accurate to at least $O(h^{k+l+2})$.

We will now review a few discontinuity detecting methods to identify troubled cells. Numerical examples to compare them will be given in the next section.

1. *The minmod-based TVB limiter* [5]. Denote

$$u^-_{i+1/2} = u_i^{(0)} + \tilde{u}_i, \qquad u^+_{i-1/2} = u_i^{(0)} - \tilde{\tilde{u}}_i.$$

From (2.2) we can see that

$$\tilde{u}_i = \sum_{l=1}^{k} u_i^{(l)} v_l^{(i)}(x_{i+1/2}), \qquad \tilde{\tilde{u}}_i = -\sum_{l=1}^{k} u_i^{(l)} v_l^{(i)}(x_{i-1/2}).$$

These are modified either by the standard minmod limiter [8]

$$\tilde{u}_i^{(mod)} = m(\tilde{u}_i, \Delta_+ u_i^{(0)}, \Delta_- u_i^{(0)}), \qquad \tilde{\tilde{u}}_i^{(mod)} = m(\tilde{\tilde{u}}_i, \Delta_+ u_i^{(0)}, \Delta_- u_i^{(0)}),$$

where the minmod function m is given by

$$m(a_1, a_2, \ldots, a_n) = \begin{cases} s \cdot \min_{1 \le j \le n} |a_j| & \text{if } \operatorname{sign}(a_1) = \operatorname{sign}(a_2) = \cdots = \operatorname{sign}(a_n) = s, \\ 0 & \text{otherwise,} \end{cases} \tag{2.4}$$

or by the TVB-modified minmod function [18]

$$\tilde{m}(a_1, a_2, \ldots, a_n) = \begin{cases} a_1 & \text{if } |a_1| \le Mh^2, \\ m(a_1, a_2, \ldots, a_n) & \text{otherwise,} \end{cases} \tag{2.5}$$

where $M > 0$ is a constant. The choice of M depends on the solution of the problem. For scalar problems it is possible to estimate M by the initial condition as in [5] (M is proportional to the second derivative of the initial condition at smooth extrema); however, it is more difficult to estimate M for the system case. If M is chosen too small, more cells than necessary will be identified as troubled cells, thereby increasing the computational cost; however, if M is chosen too large, spurious oscillations may appear.

2. *Moment limiter of Biswas, Devine, and Flaherty* [1]. We will denote this limiter as the BDF limiter in this paper. The moment-based limiter in [1] is given by

$$u_i^{(l),mod} = \frac{1}{2l-1}\, m\left((2l-1)u_i^{(l)}, u_{i+1}^{(l-1)} - u_i^{(l-1)}, u_i^{(l-1)} - u_{i-1}^{(l-1)}\right), \tag{2.6}$$

where m is again the minmod function (2.4). This limiter is applied adaptively. First, the highest-order moment $u^{(k)}$ is limited. Then the limiter is applied to successively lower-order moments when the next higher-order moment on the interval has been changed by the limiting. For our purpose, when the BDF limiter (2.6) is enacted (returns other than the first argument) for the highest-order moment, the cell is declared as a troubled cell and marked for further reconstruction.

3. *A modification of the moment limiter by Burbeau, Sagaut, and Bruneau* [2]. We will denote this modified moment limiter as the BSB limiter in this paper. For our purpose as a troubled-cell indicator, if both (2.6) and

$$\hat{u}_i^{(l),mod} = \frac{1}{2l-1} m\Big((2l-1)u_i^{(l)}, u_{i+1/2}^{(l-1)+} - u_i^{(l-1)}, u_i^{(l-1)} - u_{i-1/2}^{(l-1)-}\Big) \tag{2.7}$$

are enacted for the highest-order moment $u^{(k)}$, where

$$u_{i+1/2}^{(l-1)+} = u_{i+1}^{(l-1)} - (2l-1)u_{i+1}^{(l)}, \qquad u_{i-1/2}^{(l-1)-} = u_{i-1}^{(l-1)} + (2l-1)u_{i-1}^{(l)},$$

that is, if both $u_i^{(k),mod} \neq u_i^{(k)}$ and $\hat{u}_i^{(k),mod} \neq u_i^{(k)}$, then the cell is identified as a troubled cell, marked for further reconstruction.

4. *The monotonicity-preserving (MP) limiter* [22]. In [22], Suresh and Huynh designed a limiter to preserve accuracy near smooth extrema, which works well with Runge–Kutta time stepping for a class of high-order MP schemes. The interface values in these schemes are obtained by limiting a higher-order polynomial reconstruction. The key idea in that work is to distinguish between a smooth local extremum and a genuine $O(1)$ discontinuity.

For our purpose as a troubled-cell indicator, the MP limiter can be described as follows. First a median function is defined as

$$\text{median}(x, y, z) = x + m(y - x, z - x), \tag{2.8}$$

where m is again the minmod function (2.4). If

$$u_{i+1/2}^{-} \neq \text{median}(u_{i+1/2}^{-}, u_{i+1/2}^{\min}, u_{i+1/2}^{\max}), \tag{2.9}$$

where

$$u_{i+1/2}^{\min} = \max\Big[\min(u_i^{(0)}, u_{i+1}^{(0)}, u_{i+1/2}^{MD}), \min(u_i^{(0)}, u_{i+1/2}^{UL}, u_{i+1/2}^{LC})\Big],$$
$$u_{i+1/2}^{\max} = \min\Big[\max(u_i^{(0)}, u_{i+1}^{(0)}, u_{i+1/2}^{MD}), \max(u_i^{(0)}, u_{i+1/2}^{UL}, u_{i+1/2}^{LC})\Big],$$

and

$$d_i = u_{i+1}^{(0)} - 2u_i^{(0)} + u_{i-1}^{(0)}, \quad d_{i+1/2}^{M4X} = m(4d_i - d_{i+1}, 4d_{i+1} - d_i, d_i, d_{i+1}, d_{i-1}, d_{i+2}),$$
$$u_{i+1/2}^{MD} = \frac{1}{2}\left(u_i^{(0)} + u_{i+1}^{(0)} - d_{i+1/2}^{M4X}\right), \quad u_{i+1/2}^{UL} = u_i^{(0)} + \alpha\Big(u_i^{(0)} - u_{i-1}^{(0)}\Big),$$
$$u_{i+1/2}^{LC} = u_i^{(0)} + \frac{1}{2}\left(u_i^{(0)} - u_{i-1}^{(0)}\right) + \frac{\beta}{3} d_{i-1/2}^{M4X},$$

or if $u^+_{i-1/2}$ satisfies a similar (symmetric) condition, then the cell is identified as a troubled cell, marked for further reconstruction. We take the parameters $\alpha = 2$ and $\beta = 4$ in the numerical tests in the next section, as suggested in [22].

5. *A modification of the MP limiter* [17]. We will denote this modified MP limiter as the MMP limiter in this paper. In [17], Rider and Margolin presented a simple modification of the standard MP limiter in [22]. These modified MP limiters relax the relatively stringent condition of preserving monotonicity, while enforcing less-restrictive conditions. For our purpose as a troubled-cell indicator, the MMP limiter can be described as follows:

$$\phi = \min(1, \Delta\overline{u}^{\min}/\Delta_{\min}u), \tag{2.10}$$

where

$$\Delta\overline{u}^{\min} = u_i^{(0)} - \min\Big(u_{i-1}^{(0)}, u_i^{(0)}, u_{i+1}^{(0)}\Big), \quad \Delta_{\min}u = u_i^{(0)} - \min\big(u^+_{i-1/2}, u^-_{i+1/2}\big).$$

When $\phi \neq 1$, the limiter enacts and the cell is identified as a troubled cell, marked for further reconstruction.

6. *A shock-detection technique by Krivodonova et al. in* [12]. We will denote the troubled-cell indicator based on this technique as the KXRCF indicator in this paper.

   The strategy in [12] is based on a strong superconvergence at the outflow boundary of each element in smooth regions for the DG method to detect discontinuities and to lower the order of accuracy in the approximation there to avoid spurious oscillations near such discontinuities when solving hyperbolic systems of conservation laws.

   For our purpose as a troubled-cell indicator, the KXRCF indicator can be described as follows. Partition the boundary of a cell I_i into two portions ∂I_i^- and ∂I_i^+, where the flow is into ($\vec{v}\cdot\vec{n} < 0$) and out of ($\vec{v}\cdot\vec{n} > 0$) I_i, respectively. The discontinuity detector in [12] is defined as

$$\mathcal{I}_i = \frac{\left| \displaystyle\int_{\partial I_i^-} (u^h|_{I_i} - u^h|_{I_{n_i}})\, ds \right|}{h^{(k+1)/2} \left|\partial I_i^-\right| \|u^h|_{I_i}\|}. \tag{2.11}$$

   Here we choose h as the radius of the circumscribed circle in the element I_i, I_{n_i} is the neighbor of I_i on the side of ∂I_i^-, and the norm is based on the maximum norm taken at the integration quadrature points in two dimensions and based on an element average in one dimension. If $\mathcal{I}_i > 1$, the cell I_i is identified as a troubled cell, marked for further reconstruction.

7. *A troubled-cell indicator based on Harten's subcell resolution idea* [9]. We will denote this indicator as the Harten indicator in this paper.

   In [9], Harten introduced the notion of subcell resolution, which is based on the observation that, unlike point values, cell averages of a discontinuous piecewise-smooth function contain information about the exact location of a discontinuity within the cell. For our purpose as a troubled-cell indicator, the Harten indicator can be described as follows.

   Let

$$F_i(z) = \frac{1}{\Delta x}\left\{ \int_{x_{i-1/2}}^{z} u^h(x,t)|_{I_{i-1}} dx + \int_{z}^{x_{i+1/2}} u^h(x,t)|_{I_{i+1}} dx \right\} - u_i^{(0)},$$

where $u^h(x,t)|_{I_{i-1}}$ denotes the approximate solution u^h defined in the cell I_{i-1}, extended into cell I_i, and likewise $u^h(x,t)|_{I_{i+1}}$ is the approximate solution u^h defined in the cell I_{i+1}, extended into cell I_i. When

$$F_i(x_{i-1/2}) \cdot F_i(x_{i+1/2}) \le 0,$$

I_i is suspected of having a discontinuity of $u^h(x,t)$ in its interior. However, this could also be a smooth extremum of the solution. To exclude the latter case, Harten [9] has a criterion comparing a minmod function of the first divided differences. We modify this criterion in the context of the RKDG method as follows. We compare the kth moment $u_i^{(k)}$, which has the same magnitude of the kth derivative of $u^h(x,t)$ modulo constant with that of the neighbors. Thus, if

(2.12)
$$F_i(x_{i-1/2}) \cdot F_i(x_{i+1/2}) \le 0 \quad \text{and} \quad |u_i^{(k)}| > \alpha |u_{i-1}^{(k)}|, \quad |u_i^{(k)}| > \alpha |u_{i+1}^{(k)}|,$$

then the cell I_i is identified as a troubled cell, marked for further reconstruction. We take the constant $\alpha = 1.5$ in the numerical tests in the next section.

Once the troubled cells are identified with one of the previous seven methods, we would reconstruct the polynomial solution in this cell, while retaining its cell average using the WENO methodology [13]. We refer to [13] for the details of this reconstruction and will not repeat them here. For the case of hyperbolic systems, to identify the troubled cells, we could use either a componentwise indicator or a characteristic one. The former works on each component of the solution and identifies a troubled cell when any component of the solution is flagging this cell as a troubled cell. The latter works in the local characteristic direction to do this identification. The componentwise indicator is less expensive to implement but may identify more cells as troubled cells, thereby increasing the cost on the reconstruction in these cells. In this paper we will only show results using the componentwise indicator. We have also implemented the characteristic indicator and have obtained qualitatively similar comparison results. For both the one-dimensional and two-dimensional Euler equations, we use only the components of density and energy as indicator variables. We emphasize that the componentwise strategy is used only to identity troubled cells. Once these cells are identified, the WENO reconstructions in them are performed in local characteristic directions. We again refer to [13] and [19] for more details of the reconstruction.

3. Numerical results. In this section we perform extensive numerical experiments to compare the seven different troubled-cell indicators outlined in the previous section when used on the RKDG methods with the WENO reconstruction limiters. The comparison is concentrated on whether the results are oscillatory and on the percentage of cells flagged as troubled cells. We only plot cell averages of the solution in the graphs. The notation TVB-1, TVB-2, and TVB-3 refer to the minmod TVB limiter with the TVB constants $M = 0.01$, $M = 10$, and $M = 100$, respectively.

Example 3.1. We solve the following one-dimensional nonlinear system of Euler equations:

(3.1)
$$u_t + f(u)_x = 0$$

with

$$u = (\rho, \rho v, E)^T, \qquad f(u) = (\rho v, \rho v^2 + p, v(E+p))^T.$$

TABLE 3.1
Average and maximum percentages of cells flagged as troubled cells subject to different troubled-cell indicators for the Sod problem, and the quality of the solutions.

N	Schemes indicator	P^1			P^2			P^3		
		Ave	Max	Osc	Ave	Max	Osc	Ave	Max	Osc
200	TVB-1	10.12	23.00		11.41	23.00		13.70	23.50	
	TVB-2	0.94	2.50		1.25	3.00		1.53	3.00	
	BDF	6.24	12.00		15.89	24.50		13.15	21.50	
	BSB	5.91	11.00		13.56	19.00		14.08	21.00	
	MP	29.34	41.00		25.54	40.00		30.46	46.00	
	MMP	12.28	20.00	L	9.31	18.50		9.72	20.50	
	KXRCF	1.15	2.50		2.05	3.00		2.34	5.50	
	Harten	4.16	10.50		1.00	3.50		2.10	8.50	
400	TVB-1	8.52	17.00		10.16	20.50		11.24	20.75	
	TVB-2	0.79	1.75		0.95	2.25		1.55	2.75	
	BDF	5.46	10.00		13.40	21.25		10.64	19.50	
	BSB	5.27	8.75		10.43	14.75		10.87	16.00	
	MP	18.62	28.75		17.70	28.75		21.65	36.25	
	MMP	9.17	15.75	L	7.48	14.50		8.38	16.50	
	KXRCF	0.89	1.50		1.31	2.25		1.51	3.00	
	Harten	3.31	7.50		0.51	2.00		1.54	5.25	

Here ρ is the density, v is the velocity, E is the total energy, p is the pressure, related to the total energy by $E = \frac{p}{\gamma-1} + \frac{1}{2}\rho v^2$ with $\gamma = 1.4$.

We use the following Riemann initial condition for the Sod problem:

$$(\rho, v, p) = (1, 0, 1) \text{ for } x \le 0, \qquad (\rho, v, p) = (0.125, 0, 0.1) \text{ for } x > 0.$$

Average (over time steps) and maximum percentages of cells being flagged as troubled cells and the quality of the approximation with respect to spurious oscillations, for the different troubled-cell indicators, are summarized in Table 3.1 for $t = 2.0$ using $N = 200$ and $N = 400$ uniform cells. The quality of the approximation is marked in the column "Osc" with "Y" indicating the result is oscillatory (there exist overshoots or undershoots with a size more than 2% of the range of the exact or reference solution), "L" indicating the result is slightly oscillatory (there exist overshoots or undershoots with a size between 0.5% and 2% of the range of the exact or reference solution), or blank indicating the result is nonoscillatory (there are no overshoots or undershoots with a size more than 0.5% of the range of the exact or reference solution). We observe from Table 3.1 that the winners for this example, in terms of having smaller percentages of troubled cells, are the TVB-2, KXRCF, and Harten indicators. We can also observe that the percentage of troubled cells decreases with a mesh refinement in almost all the cases, which is a very desirable property for troubled-cell indicators.

In Figures 3.1–3.3, we plot the computed densities ρ at $t = 2.0$ against the exact solution by the RKDG method with WENO limiters using the TVB-2, KXRCF, and Harten troubled-cell indicators with $N = 200$ uniform cells for $k = 1$, 2, and 3 (second-, third-, and fourth-order RKDG). We can observe that the results for all the cases keep sharp discontinuities and are mostly oscillation-free.

Example 3.2. We repeat the numerical experiments of the previous example using the following Riemann initial condition for the Lax problem:

$$(\rho, v, p) = (0.445, 0.698, 3.528) \text{ for } x \le 0, \qquad (\rho, v, p) = (0.5, 0, 0.571) \text{ for } x > 0.$$

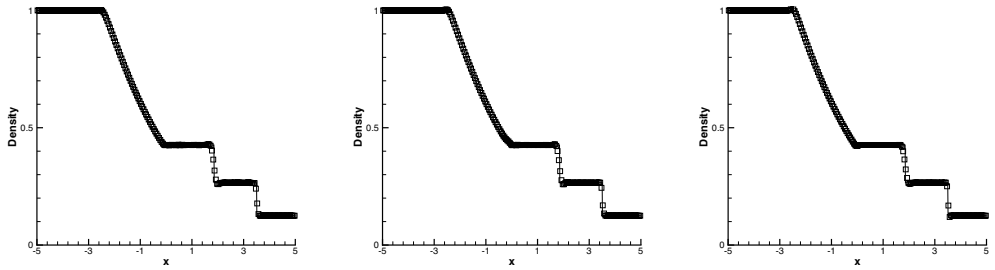

FIG. 3.1. *Sod problem, $t = 2.0$. RKDG with WENO limiters using different troubled-cell indicators: TVB-2 (left), KXRCF (middle), and Harten (right); $k = 1$, 200 cells. Density: solid line, the exact solution; squares, numerical solution.*

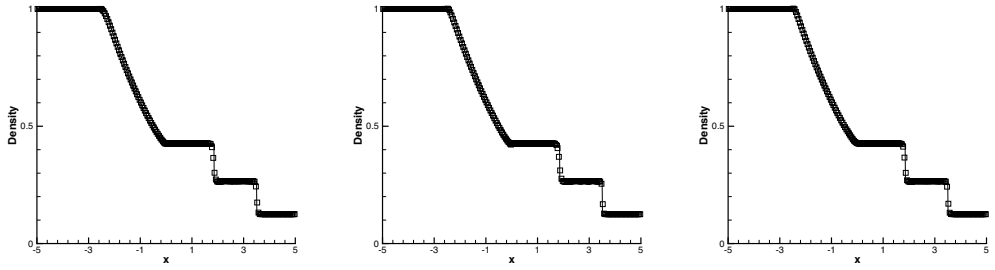

FIG. 3.2. *Sod problem, $t = 2.0$. RKDG with WENO limiters using different troubled-cell indicators: TVB-2 (left), KXRCF (middle), and Harten (right); $k = 2$, 200 cells. Density: solid line, the exact solution; squares, numerical solution.*

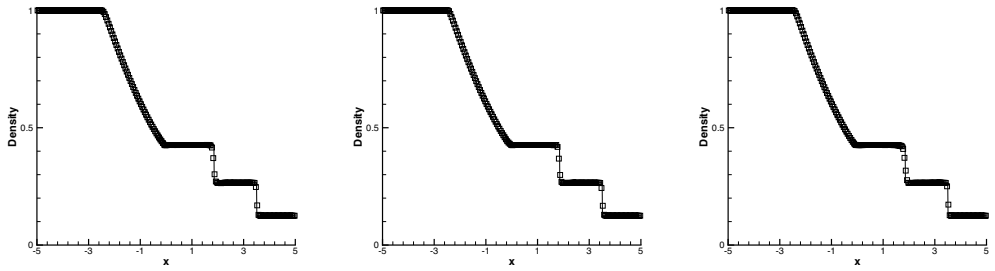

FIG. 3.3. *Sod problem, $t = 2.0$. RKDG with WENO limiters using different troubled-cell indicators: TVB-2 (left), KXRCF (middle), and Harten (right); $k = 3$, 200 cells. Density: solid line, the exact solution; squares, numerical solution.*

This is a more demanding test case in terms of controlling spurious oscillations. Results similar to those in the previous example, at $t = 1.3$, are given in Table 3.2 and in Figures 3.4–3.6. We can observe a similar pattern as in the previous example, except that more cases involving the TVB-2, MMP, KXRCF, and Harten troubled-cell indicators are marked as "slightly oscillatory" or even "oscillatory."

TABLE 3.2

Average and maximum percentages of cells flagged as troubled cells subject to different troubled-cell indicators for the Lax problem, and the quality of the solutions.

N	Schemes indicator	P^1			P^2			P^3		
		Ave	Max	Osc	Ave	Max	Osc	Ave	Max	Osc
200	TVB-1	10.68	22.00		12.70	24.00		16.31	29.00	
	TVB-2	1.87	4.50		2.56	5.50		3.87	5.50	L
	BDF	8.75	17.00		21.52	39.00		19.53	33.00	
	BSB	8.22	17.00		20.73	36.00		21.62	33.00	
	MP	28.61	36.50		27.95	41.00		32.54	41.50	
	MMP	13.24	22.00	Y	11.05	22.50	L	11.97	21.50	L
	KXRCF	1.33	3.00	L	2.10	3.50		2.46	4.50	
	Harten	3.85	9.00	L	1.00	5.00	L	2.07	6.50	L
400	TVB-1	8.55	17.50		11.02	21.75		13.66	26.00	
	TVB-2	1.37	2.75		1.82	3.50		3.29	4.50	
	BDF	7.86	15.75		19.29	36.75		17.09	34.00	
	BSB	6.57	12.50		18.96	35.50		16.23	24.75	
	MP	16.94	25.50		17.71	28.25		18.94	26.00	
	MMP	9.87	19.00	Y	9.06	18.25	L	9.23	17.00	L
	KXRCF	0.98	1.75	L	1.36	2.75		1.70	3.25	
	Harten	2.51	6.00		0.59	2.75		1.47	6.00	

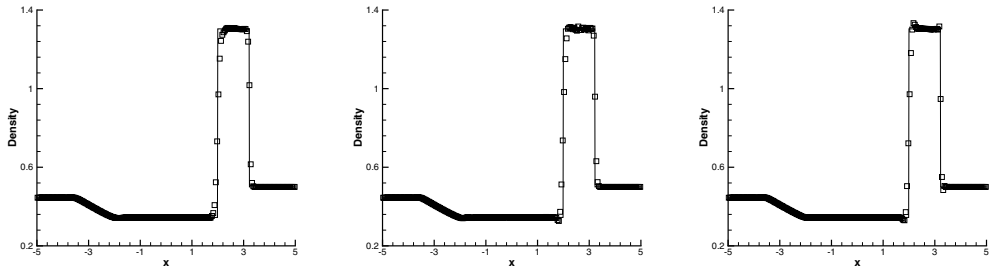

FIG. 3.4. *Lax problem, $t = 1.3$. RKDG with WENO limiters using different troubled-cell indicators: TVB-2 (left), KXRCF (middle), and Harten (right); $k = 1$, 200 cells. Density: solid line, the exact solution; squares, numerical solution.*

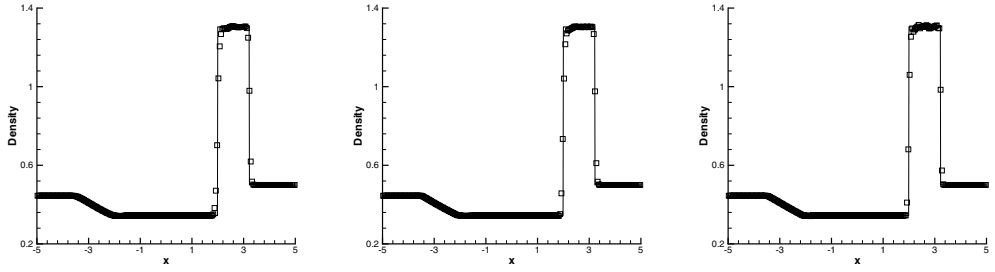

FIG. 3.5. *Lax problem, $t = 1.3$. RKDG with WENO limiters using different troubled-cell indicators: TVB-2 (left), KXRCF (middle), and Harten (right); $k = 2$, 200 cells. Density: solid line, the exact solution; squares, numerical solution.*

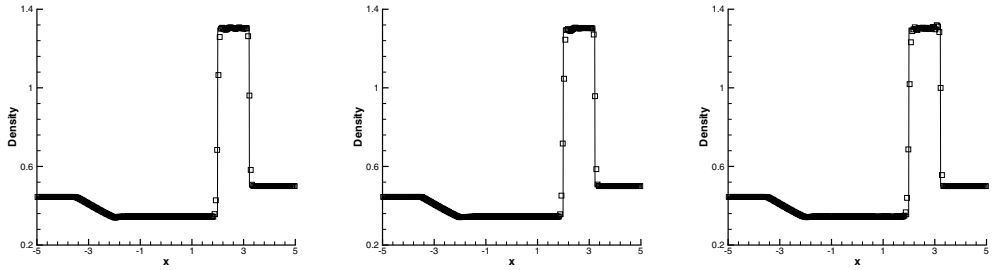

FIG. 3.6. *Lax problem, $t = 1.3$. RKDG with WENO limiters using different troubled-cell indicators: TVB-2 (left), KXRCF (middle), and Harten (right); $k = 3$, 200 cells. Density: solid line, the exact solution; squares, numerical solution.*

TABLE 3.3

Average and maximum percentages of cells flagged as troubled cells subject to different troubled-cell indicators for the shock density wave interaction problem, and the quality of the solutions.

N	Schemes indicator	P^1			P^2			P^3		
		Ave	Max	Osc	Ave	Max	Osc	Ave	Max	Osc
200	TVB-1	14.25	22.50		17.39	25.50		18.52	28.00	
	TVB-3	2.15	5.50		4.20	10.00		5.00	11.50	
	BDF	12.91	22.50		34.13	53.50		36.62	55.00	
	BSB	10.36	15.50		29.43	47.00		37.04	61.50	
	MP	25.09	35.00		22.29	35.00		27.79	39.50	
	MMP	16.82	22.00	L	14.33	21.00		14.17	19.00	L
	KXRCF	2.20	3.50		2.50	4.50		3.26	6.50	
	Harten	3.47	8.50		1.50	6.00		3.39	11.00	
400	TVB-1	9.41	16.50		10.34	15.00		10.61	15.25	
	TVB-3	2.44	6.25		3.61	9.00		3.81	8.50	
	BDF	8.81	15.75		22.31	37.75		19.15	42.00	
	BSB	7.71	11.50		18.62	36.00		21.66	45.75	
	MP	14.68	20.00		13.70	17.50		17.36	21.50	
	MMP	9.98	15.00	L	7.53	11.50		7.28	10.25	L
	KXRCF	1.31	2.25		1.51	3.25		2.31	5.00	
	Harten	1.44	3.75		0.72	3.25		2.37	8.75	

Example 3.3. A higher-order scheme would show its advantage when the solution contains both shocks and complex smooth regions. A typical example for this is the problem of shock interaction with entropy waves [21]. We solve the Euler equations (3.1) with a moving Mach = 3 shock interacting with sine waves in density, i.e., initially

$$(\rho, v, p) = (3.857143, 2.629369, 10.333333) \text{ for } x < -4,$$
$$(\rho, v, p) = (1 + \varepsilon \sin(5x), 0, 1) \text{ for } x \geq -4.$$

Here we take $\varepsilon = 0.2$. The computed density ρ is plotted at $t = 1.8$ against the reference "exact" solution, computed using a fifth-order WENO scheme [11] using 2000 grid points.

Results similar to the previous two examples, at $t = 1.8$, are given in Table 3.3 and in Figures 3.7–3.9. We can observe a similar pattern as in the previous examples; namely, the winners for this example, in terms of having smaller percentages of troubled cells, are the TVB-3, KXRCF, and Harten indicators. Notice that some cases with the MMP troubled-cell indicator are marked as "slightly oscillatory." Because

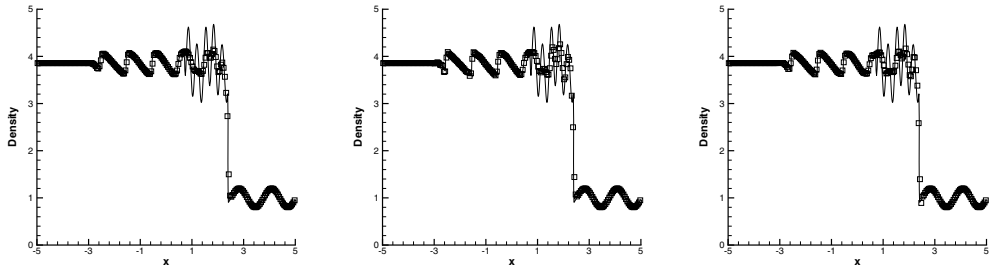

FIG. 3.7. *The shock density wave interaction problem, $t = 1.8$. RKDG with WENO limiters using different troubled-cell indicators: TVB-3 (left), KXRCF (middle), and Harten (right); $k = 1$, 200 cells. Density: solid line, the reference "exact" solution; squares, numerical solution.*

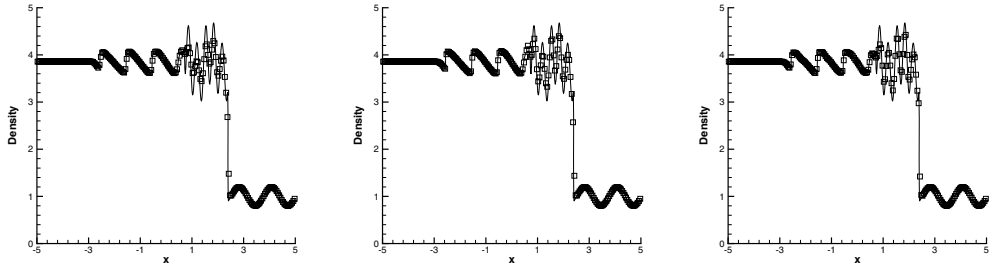

FIG. 3.8. *The shock density wave interaction problem, $t = 1.8$. RKDG with WENO limiters using different troubled-cell indicators: TVB-3 (left), KXRCF (middle), and Harten (right); $k = 2$, 200 cells. Density: solid line, the reference "exact" solution; squares, numerical solution.*

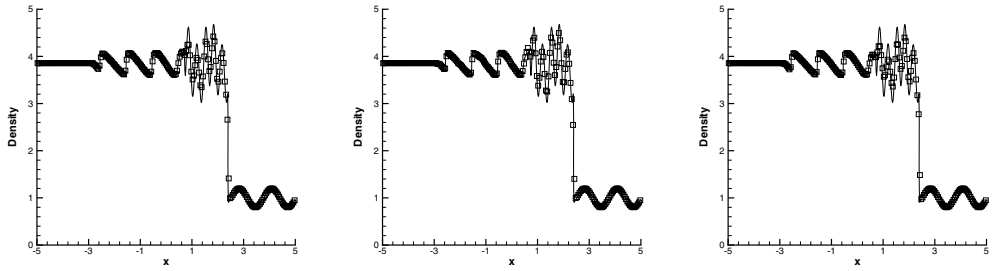

FIG. 3.9. *The shock density wave interaction problem, $t = 1.8$. RKDG with WENO limiters using different troubled-cell indicators: TVB-3 (left), KXRCF (middle), and Harten (right); $k = 3$, 200 cells. Density: solid line, the reference "exact" solution; squares, numerical solution.*

the TVB-3 and KXRCF troubled-cell indicators identify a smaller percentage of troubled cells than the Harten indicator for this problem, the resolution of the detailed structures in the solution behind the shock is better for the results using the TVB-3 and KXRCF indicators than that using the Harten indicator. This also indicates that the original RKDG method does a better job than the WENO reconstruction in

TABLE 3.4

Average and maximum percentages of cells flagged as troubled cells subject to different troubled-cell indicators for the blast wave problem, and the quality of the solutions.

N	Schemes indicator	P^1			P^2			P^3		
		Ave	Max	Osc	Ave	Max	Osc	Ave	Max	Osc
200	TVB-1	16.56	27.00		15.83	28.50		19.10	34.00	
	TVB-3	9.50	19.50		10.90	19.00		13.87	24.00	
	BDF	15.21	26.50		40.83	63.00		48.70	71.00	
	BSB	13.95	23.00		34.43	48.50		50.33	72.00	
	MP	22.90	38.50		21.89	41.50		24.35	41.50	
	MMP	12.98	22.50		11.46	22.00		12.76	23.50	
	KXRCF	13.66	23.50		15.29	22.50		20.17	29.00	
	Harten	3.59	9.50		1.67	7.00		3.66	11.00	
400	TVB-1	11.07	19.50		11.47	24.25		13.53	26.00	
	TVB-3	6.90	11.75		8.30	15.25		10.04	17.25	
	BDF	10.24	20.25		35.10	51.75		43.08	69.25	
	BSB	9.88	15.50		28.30	41.25		41.74	61.50	
	MP	14.22	25.25		15.41	26.75		17.87	31.75	
	MMP	8.69	14.00		9.08	16.50	L	8.68	18.25	L
	KXRCF	8.45	14.00		10.16	13.75		14.24	20.50	
	Harten	2.11	5.50		0.97	3.50		3.03	8.75	

keeping the resolution for such structures, so we should keep the number of troubled cells, hence the reconstruction, to a minimum under the nonoscillatory constraint. This will be beneficial both in saving computational costs for the reconstruction and in obtaining better resolutions from the original RKDG method.

Example 3.4. We consider the interaction of blast waves of the Euler equation (3.1) with the initial condition:

$$\begin{aligned}(\rho, v, p) &= (1, 0, 1000) \text{ for } 0 \le x < 0.1,\\ (\rho, v, p) &= (1, 0, 0.01) \text{ for } 0.1 \le x < 0.9,\\ (\rho, v, p) &= (1, 0, 100) \text{ for } 0.9 \le x.\end{aligned}$$

A reflecting boundary condition is applied to both ends; see [24, 10]. The computed density ρ is plotted at $t = 0.038$ against the reference "exact" solution, which is a converged solution computed by the fifth-order finite difference WENO scheme [11] with 2000 grid points.

Results similar to the previous examples, at $t = 0.038$, are given in Table 3.4 and in Figures 3.10–3.12. We can observe a similar pattern as in the previous examples; namely, the winners for this example, in terms of having smaller percentages of troubled cells, are still the TVB-3, KXRCF, and Harten indicators. For this problem, only a few cases with the MMP troubled-cell indicators are marked as "slightly oscillatory." Unlike in the previous example, in this example the Harten indicator identifies a smaller percentage of troubled cells than the TVB-3 and KXRCF indicators. As a result, the resolution is better for the results using the Harten indicator than that using the TVB-3 and KXRCF indicators, especially for the $k = 1$ (second-order) case.

Example 3.5. Double Mach reflection. This problem is originally from [24]. The computational domain for this problem is $[0, 4] \times [0, 1]$. The reflecting wall lies at the bottom, starting from $x = \frac{1}{6}$. Initially a right-moving Mach 10 shock is positioned at $x = \frac{1}{6}, y = 0$ and makes a 60° angle with the x-axis. For the bottom boundary, the exact postshock condition is imposed for the part from $x = 0$ to $x = \frac{1}{6}$ and a reflective

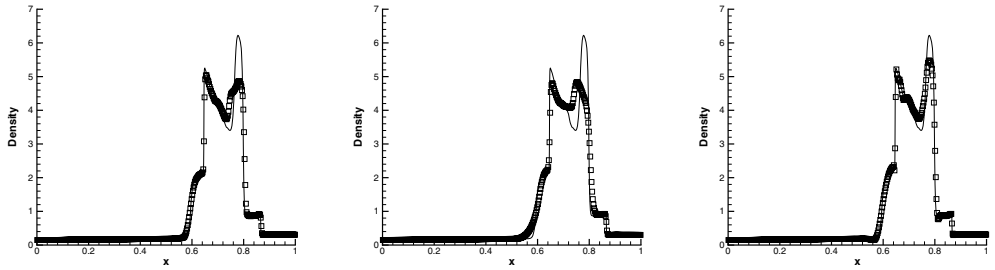

FIG. 3.10. *The blast wave problem, $t = 0.038$. RKDG with WENO limiters using different troubled-cell indicators: TVB-3 (left), KXRCF (middle), and Harten (right); $k = 1$, 400 cells. Density: solid line, the reference "exact" solution; squares, numerical solution.*

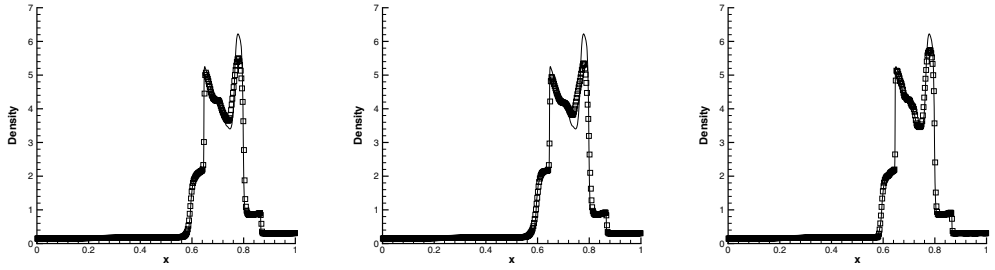

FIG. 3.11. *The blast wave problem, $t = 0.038$. RKDG with WENO limiters using different troubled-cell indicators: TVB-3 (left), KXRCF (middle), and Harten (right); $k = 2$, 400 cells. Density: solid line, the reference "exact" solution; squares, numerical solution.*

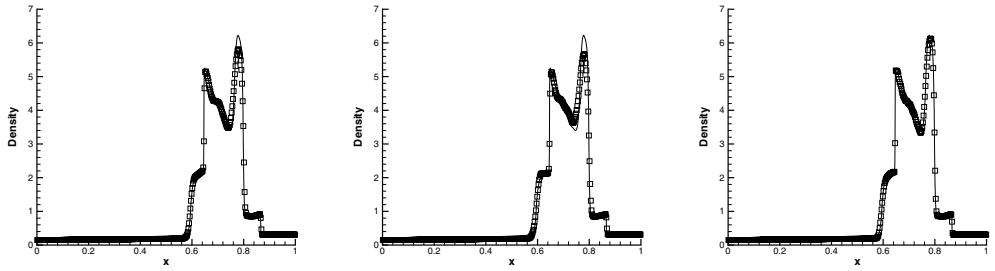

FIG. 3.12. *The blast wave problem, $t = 0.038$. RKDG with WENO limiters using different troubled-cell indicators: TVB-3 (left), KXRCF (middle), and Harten (right); $k = 3$, 400 cells. Density: solid line, the reference "exact" solution; squares, numerical solution.*

boundary condition is used for the rest. At the top boundary, the flow values are set to describe the exact motion of a Mach 10 shock. We compute the solution up to $t = 0.2$. In Table 3.5 we document the percentage of cells declared to be troubled cells for different orders of accuracy with the TVB-3, KXRCF, and Harten indicators to identify troubled cells. We can see that in most cases only a small percentage

TABLE 3.5

Average and maximum percentages of cells flagged as troubled cells subject to different troubled-cell indicators for the double Mach reflection problem.

$N_x \times N_y$	Schemes indicator	P^1		P^2		P^3	
		Average	Maximal	Average	Maximal	Average	Maximal
120×30	TVB-3	2.53	5.19	2.84	7.00	2.88	5.94
	KXRCF	6.92	9.47	11.28	17.64	12.32	19.58
	Harten	8.65	15.08	6.98	13.94	16.91	33.64
240×60	TVB-3	2.04	3.95	2.72	5.95	3.58	6.78
	KXRCF	4.65	6.51	7.49	11.99	8.45	14.65
	Harten	4.69	8.25	4.08	8.53	13.33	27.51
480×120	TVB-3	1.49	3.05	2.40	4.93	3.96	6.95
	KXRCF	2.99	4.31	4.93	7.86	7.65	12.69
	Harten	2.60	4.87	2.42	5.25	11.19	23.45
960×240	TVB-3	1.06	2.11	2.74	4.76	5.44	8.82
	KXRCF	1.85	2.73	3.44	5.40	7.80	13.10
	Harten	1.52	2.82	1.47	3.43	10.27	21.62

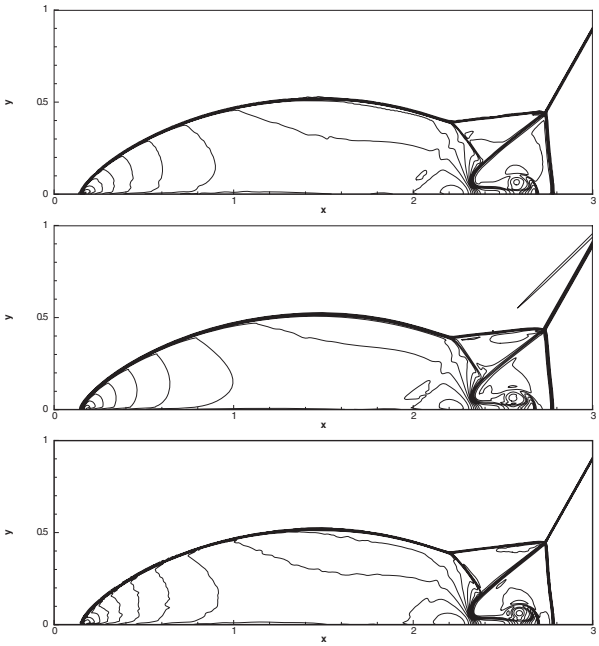

FIG. 3.13. *Double Mach reflection problem, $t = 0.2$. RKDG with WENO limiters using different troubled-cell indicators: TVB-3 (top), KXRCF (middle), and Harten (bottom); $k = 1$, 960×240 cells. Thirty equally spaced density contours from 1.5 to 22.7.*

of cells are declared as troubled cells. For this problem, the TVB-3 indicator seems to be better (in terms of producing a smaller percentage of troubled cells) than the KXRCF indicator, which in turn is better than the Harten indicator. Four uniform meshes, with 120×30, 240×60, 480×120, and 960×240 uniform cells, and three different orders of accuracy for the RKDG with WENO limiters, from $k = 1$ to $k = 3$ (second- to fourth-order), are used in the numerical experiments. To save space, we plot only the simulation results on the most refined mesh with 960×240 cells with the TVB-3, KXRCF, and Harten indicators to identify troubled cells in Figures 3.13,

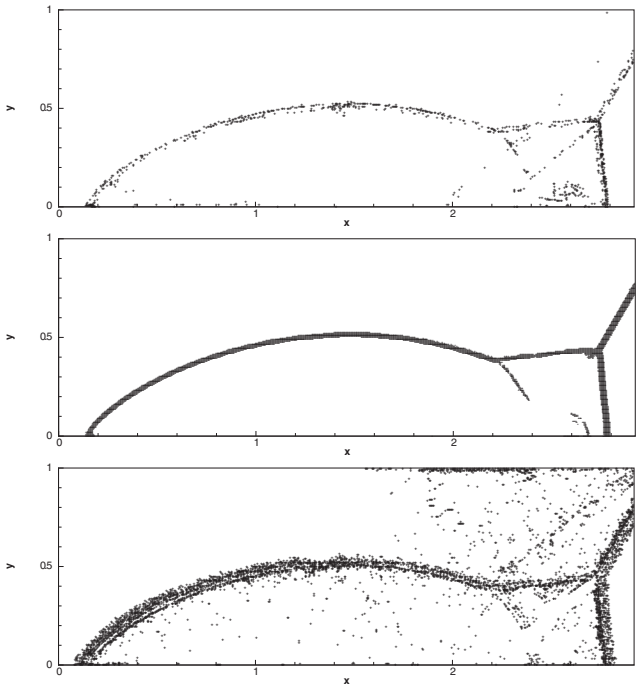

FIG. 3.14. *Double Mach reflection problem. Cells which are identified as troubled cells at* $t = 0.2$. *RKDG with WENO limiters using different troubled-cell indicators: TVB-*3 (*top*), *KXRCF* (*middle*), *and Harten* (*bottom*); $k = 1$, 960×240 *cells.*

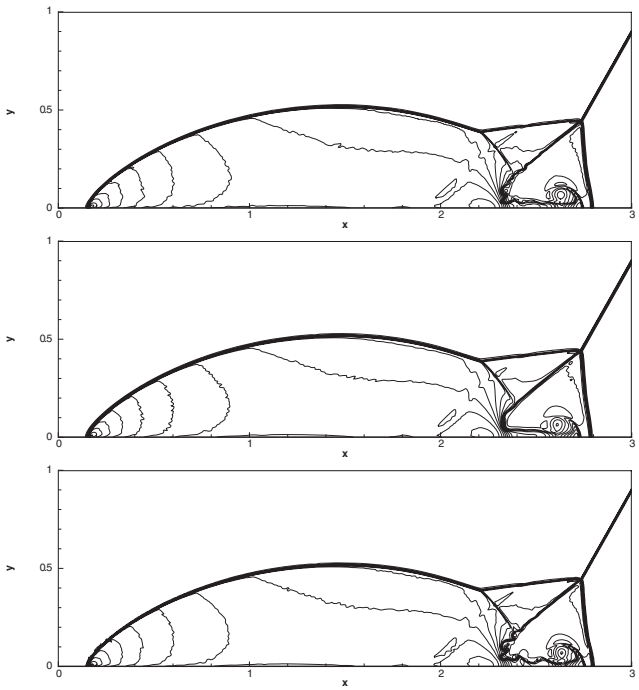

FIG. 3.15. *Double Mach reflection problem,* $t = 0.2$. *RKDG with WENO limiters using different troubled-cell indicators: TVB-*3 (*top*), *KXRCF* (*middle*), *and Harten* (*bottom*); $k = 2$, 960×240 *cells. Thirty equally spaced density contours from* 1.5 *to* 22.7.

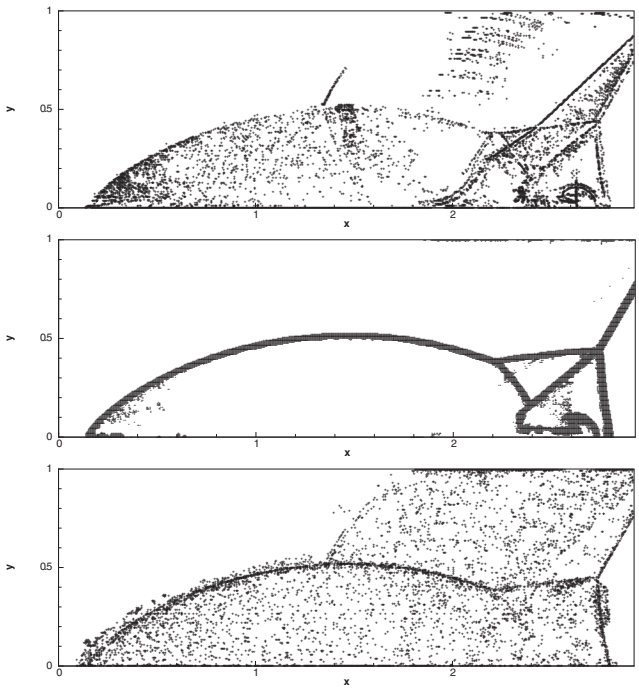

FIG. 3.16. *Double Mach reflection problem. Cells which are identified as troubled cells at* $t = 0.2$. *RKDG with WENO limiters using different troubled-cell indicators: TVB-3 (top), KXRCF (middle), and Harten (bottom);* $k = 2$, 960×240 *cells.*

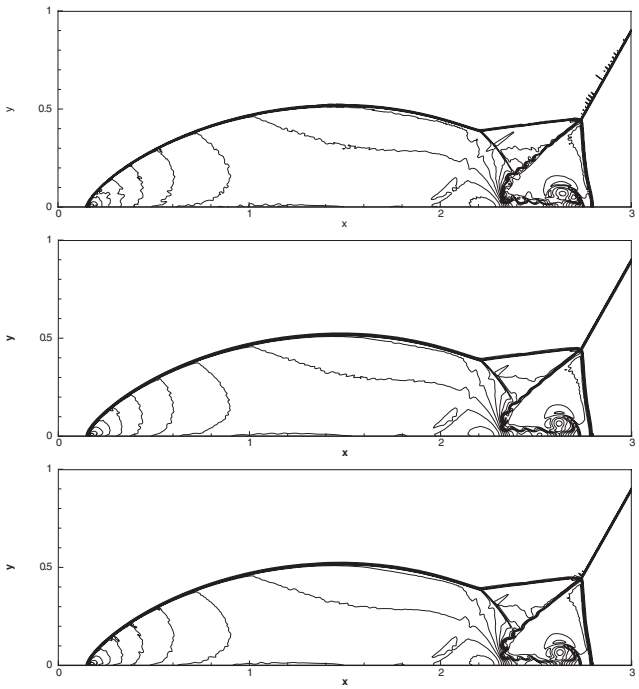

FIG. 3.17. *Double Mach reflection problem,* $t = 0.2$. *RKDG with WENO limiters using different troubled-cell indicators: TVB-3 (top), KXRCF (middle), and Harten (bottom);* $k = 3$, 960×240 *cells. Thirty equally spaced density contours from* 1.5 *to* 22.7.

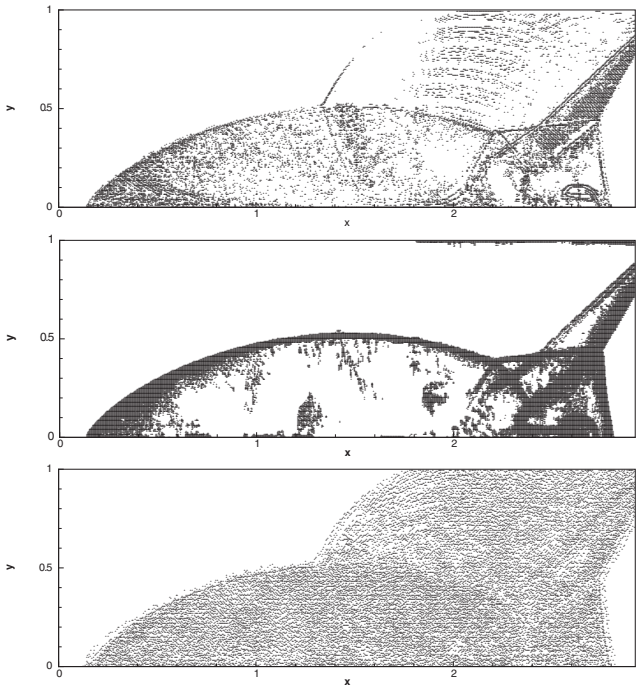

FIG. 3.18. *Double Mach reflection problem. Cells which are identified as troubled cells at* $t = 0.2$. *RKDG with WENO limiters using different troubled-cell indicators: TVB-*3 (*top*), *KXRCF* (*middle*), *and Harten* (*bottom*); $k = 3$, 960×240 *cells.*

3.15, and 3.17. All the figures are showing 30 equally spaced density contours from 1.5 to 22.7. The troubled cells identified by the TVB-3, KXRCF, and Harten indicators at the last time step are shown in Figures 3.14, 3.16, and 3.18, respectively. It is intriguing to see, in Figures 3.13–3.18, that raising the order of approximation from second- to fourth-order (from $k = 1$ to $k = 3$) leads to an increase in the number of troubled cells. Also, the extent to which the three troubled-cell indicators give the correct identification of the troubled cells affects not only the number but also the distribution of the troubled cells within the computational domain, as k increases from 1 to 3.

4. Concluding remarks. In this paper we have systematically studied and compared a few different troubled-cell indicators for the RKDG methods using WENO methodology as limiters. Extensive one- and two-dimensional simulations on the hyperbolic systems of Euler equations indicate that the minmod-based TVB indicator (when the TVB constant M is suitably chosen), the KXRCF indicator by Krivodonova et al. [12], and an indicator based on Harten's subcell resolution idea [9] are better than other choices in all the test cases. Among these three there is no clear winner: any one of them would work better in some examples but not in all examples. All three of them should be suitable candidates for applications of the RKDG methods using WENO reconstructions.

Acknowledgments. The first author would like to thank Professor B. C. Khoo and Professor G. W. Wei for their support and help.

REFERENCES

[1] R. Biswas, K.D. Devine, and J. Flaherty, *Parallel, adaptive finite element methods for conservation laws*, Appl. Numer. Math., 14 (1994), pp. 255–283.

[2] A. Burbeau, P. Sagaut, and C.H. Bruneau, *A problem-independent limiter for high-order Runge–Kutta discontinuous Galerkin methods*, J. Comput. Phys., 169 (2001), pp. 111–150.

[3] B. Cockburn, S. Hou, and C.-W. Shu, *The Runge–Kutta local projection discontinuous Galerkin finite element method for conservation laws* IV: *The multidimensional case*, Math. Comp., 54 (1990), pp. 545–581.

[4] B. Cockburn, S.-Y. Lin, and C.-W. Shu, *TVB Runge–Kutta local projection discontinuous Galerkin finite element method for conservation laws* III: *One dimensional systems*, J. Comput. Phys., 84 (1989), pp. 90–113.

[5] B. Cockburn and C.-W. Shu, *TVB Runge–Kutta local projection discontinuous Galerkin finite element method for conservation laws* II: *General framework*, Math. Comp., 52 (1989), pp. 411–435.

[6] B. Cockburn and C.-W. Shu, *The Runge–Kutta local projection $P1$-discontinuous Galerkin finite element method for scalar conservation laws*, RAIRO Modél. Math. Anal. Numér., 25 (1991), pp. 337–361.

[7] B. Cockburn and C.-W. Shu, *The Runge–Kutta discontinuous Galerkin method for conservation laws* V: *Multidimensional systems*, J. Comput. Phys., 141 (1998), pp. 199–224.

[8] A. Harten, *High resolution schemes for hyperbolic conservation laws*, J. Comput. Phys., 49 (1983), pp. 357–393.

[9] A. Harten, *ENO schemes with subcell resolution*, J. Comput. Phys., 83 (1989), pp. 148–184.

[10] A. Harten, B. Engquist, S. Osher, and S. Chakravathy, *Uniformly high order accurate essentially non-oscillatory schemes,* III, J. Comput. Phys., 71 (1987), pp. 231–303.

[11] G. Jiang and C.-W. Shu, *Efficient implementation of weighted ENO schemes*, J. Comput. Phys., 126 (1996), pp. 202–228.

[12] L. Krivodonova, J. Xin, J.-F. Remacle, N. Chevaugeon, and J.E. Flaherty, *Shock detection and limiting with discontinuous Galerkin methods for hyperbolic conservation laws*, Appl. Numer. Math., 48 (2004), pp. 323–338.

[13] J. Qiu and C.-W. Shu, *Runge–Kutta discontinuous Galerkin method using WENO limiters*, SIAM J. Sci. Comput., 26 (2005), pp. 907–929.

[14] J. Qiu and C.-W. Shu, *Hermite WENO schemes and their application as limiters for Runge–Kutta discontinuous Galerkin method: One dimensional case*, J. Comput. Phys., 193 (2003), pp. 115–135.

[15] J. Qiu and C.-W. Shu, *Hermite WENO schemes and their application as limiters for Runge–Kutta discontinuous Galerkin method* II: *Two dimensional case*, Comput. Fluids, 34 (2005), pp. 642–663.

[16] W.H. Reed and T.R. Hill, *Triangular Mesh Methods for Neutron Transport Equation*, Technical report LA-UR-73-479, Los Alamos Scientific Laboratory, Los Alamos, NM, 1973.

[17] W.J. Rider and L.G. Margolin, *Simple modifications of monotonicity-preserving limiters*, J. Comput. Phys., 174 (2001), pp. 473–488.

[18] C.-W. Shu, *TVB uniformly high-order schemes for conservation laws*, Math. Comp., 49 (1987), pp. 105–121.

[19] C.-W. Shu, *Essentially non-oscillatory and weighted essentially non-oscillatory schemes for hyperbolic conservation laws*, in Advanced Numerical Approximation of Nonlinear Hyperbolic Equations, Lecture Notes in Math. 1697, A. Quarteroni, ed., Springer, New York, 1998, pp. 325–432.

[20] C.-W. Shu and S. Osher, *Efficient implementation of essentially non-oscillatory shock-capturing schemes*, J. Comput. Phys., 77 (1988), pp. 439–471.

[21] C.-W. Shu and S. Osher, *Efficient implementation of essentially non-oscillatory shock capturing schemes* II, J. Comput. Phys., 83 (1989), pp. 32–78.

[22] A. Suresh and H.T. Huynh, *Accurate monotonicity-preserving schemes with Runge–Kutta time stepping*, J. Comput. Phys., 136 (1997), pp. 83–99.

[23] P.K. Sweby, *High resolution schemes using flux limiters for hyperbolic conservation laws*, SIAM J. Numer. Anal., 21 (1984), pp. 995–1011.

[24] P. Woodward and P. Colella, *The numerical simulation of two-dimensional fluid flow with strong shocks*, J. Comput. Phys., 54 (1984), pp. 115–173.